Engineering Geology 121 (2011) 150–164

Contents lists available at ScienceDirect

Engineering Geology

journal homepage: www.elsevier.com/locate/enggeo

Response spectral attenuation relations for shallow crustal earthquakes in Taiwan

Po-Shen Lin [a], Chyi-Tyi Lee [b,*], Chin-Tung Cheng [c], Chih-Hsuan Sung [d]

[a] Institute of Geophysics, National Central University, No.300, Jungda Road, Jungli City, Taoyuan County, 32001, Taiwan
[b] Institute of Applied Geology, National Central University, No.300, Jungda Road, Jungli City, Taoyuan County, 32001, Taiwan
[c] Geotechnical Engineering Research Center, Sinotech Engineering Consultants, Inc., Basement No.7 Lane No.26, Yat-sen Road, Taipei, 11071, Taiwan
[d] Institute of Applied Geology, National Central University, Taiwan

ARTICLE INFO

Article history:
Received 14 May 2009
Received in revised form 21 April 2011
Accepted 28 April 2011
Available online 10 May 2011

Keywords:
Attenuation relationship
Crustal earthquakes
Strong ground motion
Peak ground acceleration
Spectral acceleration
Hanging-wall effect

ABSTRACT

In this study, a local set of response spectral attenuation equations, developed for seismic hazard analysis in Taiwan, are introduced as an example for determining the local strong motion attenuation relationship for a region. Strong ground-motion data for shallow crustal earthquakes are obtained from the Taiwan Strong-motion Instrumentation Program (TSMIP). These data are used to establish peak ground acceleration (PGA) and response spectral acceleration (SA) attenuation equations taking into consideration both hanging-wall effects and site conditions. The obtained results show that the local set of attenuation equations gives significantly lower values of PGA and SA for structural periods shorter than 0.3 s as compared to a set of global relations obtained from international data. The SAs obtained for structural periods longer than 0.3 s are similar to those obtained for global sets. This indicates that developing a local set of ground-motion attenuation equations is necessary for more accurate prediction of ground motion values.

1. Introduction

A set of local response spectral attenuation equations is essential for probabilistic seismic hazard analysis (PSHA) in a specific region. The analysis should include the ground-motion for different response spectral periods, and should adequately reflect the fact that the amplitude of the ground-motion increases with earthquake magnitude and decreases as propagation distance increases.

Utmost care should be taken when developing a set of attenuation equations for practical use in PSHA. In particular, the standard deviation of the ground-motion values should not be too big, since PSHA is very sensitive to the standard deviation, whose values, if excessively large, can lead to overly-conservative ground-motion predictions (Anderson and Brune, 1999; Bommer and Abrahamson, 2006).

The development of a local set of response spectral attenuation equations is required for any place where earthquake resistant design or safety evaluation of existing structures is needed. This is definitely true of Taiwan, because high seismicity and disastrous earthquakes have already been experienced. However, there is a lack of response spectral attenuation equations for shallow crustal earthquakes in Taiwan, with the exception of those used for subduction zone earthquakes in northeastern Taiwan (Lin and Lee, 2008) and for describing the ground motion characteristics of the Chi-Chi earthquake (Loh et al., 2000a). The ready-made local attenuation equations utilized in most previous studies have only investigated PGA, and do not report standard deviation (Hwang, 1995; Liu et al., 1999; Chang et al., 2001; Wu et al., 2001). In the last twenty years, five different forms of PGA attenuation equations (four calculated by Tsai et al., 1987 and one by Loh et al., 2000b) do provide a standard deviation and are still widely used by engineering consultants in Taiwan.

The present problem in Taiwan is not only the lack of spectral attenuation, but also the inherent weakness of using just a local magnitude scale for earthquakes and the lack of consideration of site classification. For example, right after the 1999 Chi-Chi earthquake (Ma et al., 1999; Kao and Chen, 2000) it was found that, due to the 'magnitude saturation' phenomenon, the Richter magnitude scale was not appropriate for developing the ground-motion attenuation equations for PSHA and the use of the seismic moment magnitude M_W was recommended. We also need to develop attenuation equations using the closest distance from the rupture surface instead of hypocentral distance, as in the relations used until now. Furthermore, for the Chi-Chi earthquake, significant differences were found in ground-motion values between the hanging-wall and the footwall side of the fault and this is yet another point that should be reflected in the attenuation equations.

Lin and Lee (2008) established a set of response spectral attenuation equations for subduction zone earthquakes in northeastern Taiwan, using M_W and hypocentral distance. This paper introduces a set of response spectral attenuation equations for shallow crustal earthquakes in Taiwan using M_W and the closest distance from the rupture surface. This local set of attenuation equations covers

* Corresponding author. Tel.: +886 3 4253334; fax: +886 3 4223357.
E-mail addresses: person@gis.geo.ncu.edu.tw (P.-S. Lin), ct@ncu.edu.tw (C.-T. Lee), ctcheng@sinotech.org.tw (C.-T. Cheng), karen@gis.geo.ncu.edu.tw (C.-H. Sung).

0013-7952/$ – see front matter © 2011 Elsevier B.V. All rights reserved.
doi:10.1016/j.enggeo.2011.04.019

spectral periods from 0 to 5 s, and emphasizes differences in site classes and the hanging-wall effect.

2. Seismotectonics of Taiwan

The island of Taiwan is located at the boundary between the Philippine Sea plate and the Eurasian plate. The Philippine Sea plate is moving towards northwest at a rate of about 7–8 cm/yr (Seno, 1977; Seno et al., 1993; Yu et al., 1997), while the Luzon arc, at the leading edge of the Philippine Sea plate, is colliding with the Eurasian plate in eastern Taiwan. In northeastern Taiwan, the Philippine Sea plate is subducting beneath the Eurasia plate. In southwestern Taiwan, the Philippine Sea plate is obducting over the oceanic lithosphere of the South China Sea which is attached to the Eurasian plate (Fig. 1).

The arc–continent collision started in the Late Miocene (Chai, 1972; Bowin et al., 1978; Letouzey and Kimura, 1986), and has produced the highly deformed terrain of Taiwan, marked with intensely folding and thrusting. The island is experiencing active crustal deformation (Bonilla, 1975, 1977; Yu et al., 1997) and frequent earthquakes (Hsu, 1971; Tsai et al., 1977; Wu, 1978). Also, the region is affected by numerous typhoons and characterized by a high erosion rate (Dadson et al., 2003) all of which are rapid earth altering processes leading to changing landforms in the Taiwan region.

Over the last four hundred years or so, more than 130 disastrous earthquakes have occurred in and around Taiwan (Lee et al., 1976; Hsu, 1983; Tsai, 1986). Some have produced large amounts of damage, such as the 1999 Chi-Chi Taiwan earthquake of M_W 7.6 (Ma et al., 1999; Kao and Chen, 2000). The earthquakes in this seismotectonic environment may be grouped into two seismogenic categories: shallow crustal earthquakes and subduction zone earthquakes. The former are the focus of this article.

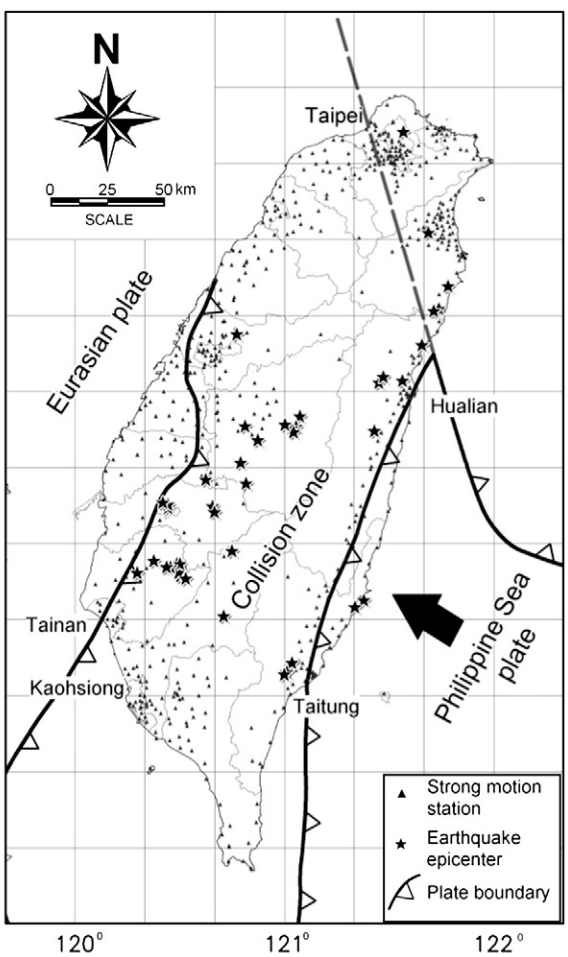

Fig. 1. Map showing the distribution of earthquake epicenters (star) used in this study and the distribution of TSMIP strong-motion stations (gray triangles).

3. Data description

Beginning in 1991, the Seismology Center of the Central Weather Bureau, Taiwan (CWB), embarked on a program known as the Taiwan Strong Motion Instrumentation Program (TSMIP) (Liu et al., 1999). The main goal of this program is to collect high quality instrumental recordings of strong earthquake shaking. These data are crucial for understanding earthquake source mechanisms, seismic wave propagation and local site effects. At the present time, there are more than 700 stations, and more than one hundred thousand high-quality 3-component digital accelerograms have been collected. These new recordings provide an excellent database for ground-motion attenuation studies (Liu, 1999; Chang et al., 2001; Wu et al., 2001; Lin and Lee, 2008).

The locations of the TSMIP stations are shown in Fig. 1. Except in the mountainous areas, these free-field stations are densely spaced approximately 5 km apart on average and only about 3 km apart in urban areas. The deployment of instruments started in 1991, with most becoming operational by December 1994. Each operating free-field station includes triaxial accelerometers, a digital recording subunit, a power supply, and a timing system.

The CWB releases information about the magnitude of each earthquake in local magnitude (M_L). However, when large magnitude earthquakes (M_L>6.5) are considered, a saturation problem arises (Heaton et al., 1986). To avoid this problem, the moment magnitude, M_W (Hanks and Kanamori, 1979), which is directly related to the fault rupture area and earthquake energy, is used as the magnitude parameter in the attenuation model discussed in the present study. We use a M_W–M_L relation developed by Tsai and Wen (1999) to convert M_L to M_W. The equation is as follows:

$$M_L = 0.193 + 0.993M_W. \tag{1}$$

Because the data used in developing this equation is from M_L 4.8 to M_L 7.1, this conversion is used only for earthquake magnitude less than or equal to M_L 6.8. For the moment magnitude of the Chi-Chi mainshock, the USGS estimate was adopted.

For strong-motion data, screening is performed on the earthquake records prior to processing. Original earthquake records are put through base line correction, and then plotted as a time history. Earthquake records are selected manually, and damaged or questionable records are excluded. Records with square waves due to the ground-motion values being too small are also disposed of. After screening, 4383 sets of 3-component data remain. Earthquake epicentres for this data set are shown also in Fig. 1, and details of earthquake parameters are listed in Table 1.

For the purpose of establishing a set of spectral attenuation equations, we calculate the 5% critical-damping ratio response spectrum for each strong-motion record, with periods ranging from 0.01 to 5 s, at sampling intervals of 0.01 s. Prior to the regression analysis, the geometric mean of the two horizontal components was used as the horizontal ground-motion value.

We use the site classification results obtained by Lee et al. (2001) to distinguish between rock (categories B and C in Lee et al., 2001) and soil sites (categories D and E in Lee et al., 2001). Considering the hanging-wall effect, the records from the Chi-Chi earthquake are divided into three groups: hanging-wall sites, footwall sites and others, as shown in Fig. 2.

Hanging-wall of a dip-slip fault is defined as the overlying side of a fault: we assumed that it extends within 30 km of the fault line and beyond the ends of the fault line within 30° from the normal to the fault strike. Footwall of a dip-slip fault is defined as the underlying side of a fault: we assume that it extends within 40 km of the fault line

Table 1
Parameters of the Taiwan earthquakes used in this study.

No.	Date	Time	Lon.	Lat.	Depth	M_L	M_W	Fault type	Rec._no.
1	1993/12/13	09:23:30	120.776	24.256	25.8	4.5	4.37	RO	28
2	1993/12/15	21:49:43	120.507	23.194	15.2	5.7	5.55	R	138
3	1993/12/20	03:32:04	120.506	23.227	17.1	4.4	4.25	SS	39
4	1993/12/21	03:14:28	120.509	23.216	18.6	4.5	4.33	R	42
5	1993/12/22	16:22:20	120.499	23.208	17.4	4.6	4.47	SS	44
6	1994/03/28	08:11:15	120.714	23.018	23.1	5.4	5.25	RO	81
7	1994/04/06	01:12:11	120.448	23.494	19.0	5.0	4.87	SS	76
8	1994/05/31	15:00:06	120.794	23.692	9.2	4.6	4.41	NO	35
9	1994/06/05	01:09:30	121.787	24.468	5.1	6.5	6.35	NO	214
10	1995/01/19	11:39:08	120.753	23.305	17.0	4.5	4.30	RO	45
11	1995/02/26	08:08:18	121.384	23.088	19.9	4.9	4.71	RO	39
12	1995/03/22	03:30:21	121.435	23.831	7.4	4.8	4.68	R	34
13	1995/04/11	17:47:27	120.504	23.248	17.3	4.1	3.92	R	31
14	1995/04/23	02:47:40	120.459	23.233	11.9	4.3	4.09	RO	33
15	1995/04/23	02:57:52	120.437	23.233	9.8	4.3	4.16	SS	40
16	1995/04/23	03:01:46	120.441	23.234	12.1	4.3	4.15	SS	45
17	1995/05/01	14:50:45	121.569	24.052	13.0	4.9	4.73	RO	30
18	1995/05/27	18:11:11	121.342	23.058	21.1	5.3	5.10	R	143
19	1995/07/07	03:04:48	121.078	23.896	15.2	5.3	5.14	R	163
20	1995/07/14	16:52:46	121.743	24.368	9.8	5.8	5.65	SS	194
21	1995/07/14	17:40:48	121.719	24.358	5.2	4.9	4.71	SS	31
22	1995/09/28	17:58:05	120.449	23.509	11.9	4.5	4.32	SS	54
23	1995/10/31	22:27:06	120.38	23.262	18.5	5.2	5.03	R	117
24	1995/11/14	07:26:26	121.456	24.044	10.3	4.2	4.05	SS	28
25	1996/04/07	16:55:36	120.67	23.475	4.4	4.7	4.54	R	45
26	1996/05/28	21:53:22	121.477	24.069	16.2	5.1	4.89	–	71
27	1996/10/19	19:16:05	120.532	23.183	16.9	4.2	4.05	R	41
28	1996/11/16	00:22:43	120.3	23.208	20.2	4.3	4.12	RO	35
29	1997/04/02	22:36:41	121.692	24.701	8.5	4.3	4.17	N	48
30	1997/06/24	16:37:12	121.573	25.143	6.9	3.7	3.53	SS	37
31	1997/09/05	12:41:06	121.04	22.813	2.0	3.7	3.54	SS	12
32	1997/10/29	23:18:37	120.628	23.618	13.3	4.3	4.16	RO	33
33	1997/11/14	04:29:50	121.662	24.209	10.2	5.4	5.24	–	53
34	1998/01/18	19:56:51	121.015	22.773	3.3	5.1	4.91	SS	54
35	1998/01/20	23:29:38	121.003	22.763	2.7	5.1	4.91	RO	34
36	1998/07/17	04:51:14	120.66	23.5	6.0	6.2	6.05	R	277
37	1999/09/20	17:47:15	120.816	23.8525	8.0	7.3	7.60	R	419
38	1999/09/20	18:03:40	120.876	23.7915	3.5	6.6	6.42	N	361
39	1999/09/20	18:11:52	121.06	23.8502	1.0	6.7	6.55	–	412
40	1999/09/20	18:16:16	121.039	23.8442	1.1	6.7	6.51	–	395
41	1999/09/20	21:46:37	120.821	23.6015	0.3	6.6	6.44	R	370
42	1999/09/22	00:14:40	121.047	23.8263	15.6	6.8	6.65	RO	388
43	1999/09/25	23:52:49	121.006	23.8593	9.9	6.8	6.65	R	305
44	1999/10/22	02:18:56	120.422	23.517	16.6	6.4	6.25	RO	67

Note: Fault type data adopted from Wu et al. (2008), classified into Strike-slip (SS), Normal fault (N), Normal-oblique fault (NO), Reverse fault (R), Reverse-oblique fault (RO), based on the rake angle. Depth is in km.

and also beyond the ends of the fault line within 30° from the normal to the fault strike. (see Fig. 2).

Since there is a lack of ground-motion data for earthquake magnitudes from 6.5 to 7.6 and distance in the near field, some data relative to large earthquakes, hanging-wall, and near field conditions are derived from similar geotectonic environment outside Taiwan to develop reliable attenuation relationships for PSHA. The data selected from international sources are listed in Table 2. In the end, we are left with four groups of data, i.e. for hanging-wall rock sites, hanging-wall soil sites, footwall rock sites, and footwall soil sites. There are a total of 52 earthquakes and 5,268 records; only 87 records (1.7%) are taken from global data set so that the developed attenuation equations still basically represent local relations. The magnitude and distance distribution are shown in Fig. 3; the value ranges for the moment magnitude are 3.5–7.6 and for distance are 1–240 km. The distance parameter used in this study is the closest distance from the rupture surface, while hypocentral distance is used for earthquakes without a finite fault model (Beresnev and Atkinson, 1999).

Most of the data are relative to earthquakes with reverse and reverse-oblique fault mechanisms and only few of them are of other

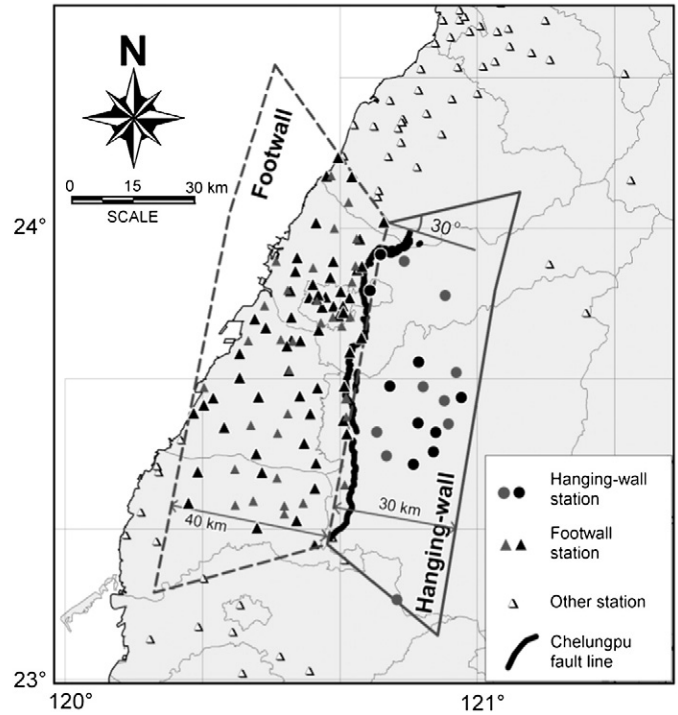

Fig. 2. Map showing the distribution of strong-motion stations around the Chelungpu fault, where full circles indicate stations on the hanging-wall side and full triangles indicate stations on the footwall side. Black circles and black triangles mean that strong-motion records from the Chi-Chi earthquake mainshock are available, whereas gray circles and gray triangles mean that records of the Chi-Chi mainshock are missing.

types (some strike-slip fault, two normal-oblique fault and two normal fault mechanisms). Thus, differences in fault types were not considered in developing our attenuation model.

With regard to hanging-wall effect, it can be generally observed only in case of dip-slip faults which rupture or deform ground surface. Among all the 44 local earthquakes, only the Chi-Chi mainshock deformed and ruptured the ground surface, therefore, only its records are used in developing the hanging-wall/footwall attenuation equations. Additionally, data relative to earthquakes outside Taiwan were used deriving hanging-wall/footwall category from related websites and/or reports.

4. Attenuation model and regression method

An attenuation relationship describes the ground-motion value expected at a site, given source characteristics, wave path, and site effects, parameterized in a simplified way. The most common

Table 2
Parameters of earthquakes of areas outside Taiwan used in this study.

No.	Date	Time	Lon.	Lat.	Depth	M_W	Rec. no.	Eq. name
1	1978/09/16	–	57.323	33.215	5.8	7.4	2	Tabas, Iran
2	1983/05/02	23:42	−120.310	36.233	4.6	6.4	5	Coalinga
3	1985/12/23	–	−124.243	62.187	8	6.8	3	Nahanni, Canada
4	1986/07/08	09:20	−116.612	34.000	11	6.0	5	N. Palm Springs
5	1987/10/01	14:42	−118.081	34.049	14.6	6.0	6	Whittier Narrows
6	1989/10/18	00:05	−121.883	37.041	17.5	6.9	7	Loma Prieta
7	1992/04/25	18:06	−124.229	40.334	9.6	7.1	2	Cape Mendocino
8	1992/06/28	11:58	−116.430	34.200	7	7.3	57	Landers

Note: The record numbers represent the number of records used in this study not the records for that earthquake. Depth is in km.

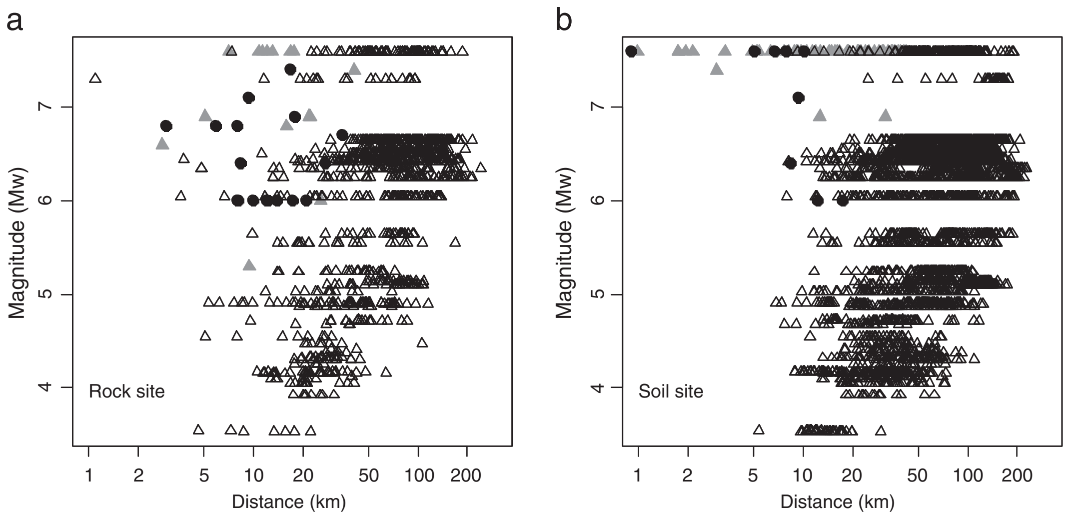

Fig. 3. Magnitude and distance distribution of the ground-motion data set used in this study: (a) rock sites; (b) soil sites. The full black circles represent data used in the hanging-wall model and full gray triangles represent data used in the footwall model. Open triangles means others (or not differentiated between hanging-wall and footwall).

Table 3
Regression coefficients of attenuations for the hanging-wall and rock sites.

Period	c_1	c_2	c_3	c_4	c_5	$\sigma_{\ln y}$
PGA	−3.279	1.035	−1.651	0.152	0.623	0.651
0.01	−3.253	1.018	−1.629	0.159	0.612	0.647
0.06	−1.738	0.908	−1.769	0.327	0.502	0.702
0.09	−1.237	0.841	−1.750	0.478	0.402	0.748
0.10	−1.103	0.841	−1.765	0.455	0.417	0.750
0.20	−2.767	0.980	−1.522	0.097	0.627	0.697
0.30	−4.440	1.186	−1.438	0.027	0.823	0.685
0.40	−5.630	1.335	−1.414	0.014	0.932	0.683
0.50	−6.746	1.456	−1.365	0.006	1.057	0.678
0.60	−7.637	1.557	−1.348	0.0033	1.147	0.666
0.75	−8.641	1.653	−1.313	0.0015	1.257	0.652
1.0	−9.978	1.800	−1.286	0.0008	1.377	0.671
1.5	−11.617	1.976	−1.284	0.0004	1.508	0.683
2.0	−12.611	2.058	−1.261	0.0005	1.497	0.706
3.0	−13.303	2.036	−1.234	0.0013	1.302	0.702
5.0	−13.914	1.958	−1.156	0.0012	1.241	0.726

Note: Regression equation $\ln(y) = c_1 + c_2 M + c_3 \ln(R + c_4 e^{C_5 M}) \pm \sigma_{\ln y}$.

Table 5
Regression coefficients of attenuations for the footwall and rock sites.

Period	c_1	c_2	c_3	c_4	c_5	$\sigma_{\ln y}$
PGA	−3.232	1.047	−1.662	0.192	0.630	0.652
0.01	−3.193	1.017	−1.612	0.210	0.590	0.648
0.06	−2.643	0.937	−1.602	0.230	0.550	0.709
0.09	−2.093	0.907	−1.642	0.230	0.550	0.755
0.10	−1.993	0.907	−1.652	0.190	0.590	0.756
0.20	−2.659	0.960	−1.512	0.148	0.610	0.699
0.30	−4.387	1.169	−1.422	0.044	0.790	0.686
0.40	−5.634	1.328	−1.399	0.022	0.900	0.682
0.50	−6.391	1.410	−1.347	0.018	0.950	0.734
0.60	−7.634	1.576	−1.345	0.0043	1.191	0.721
0.75	−8.885	1.665	−1.254	0.0009	1.394	0.701
1.0	−10.031	1.777	−1.240	0.0007	1.416	0.717
1.5	−11.633	1.930	−1.219	0.0005	1.463	0.678
2.0	−12.599	1.989	−1.174	0.0005	1.464	0.703
3.0	−13.311	1.974	−1.140	0.0009	1.306	0.701
5.0	−13.985	1.957	−1.145	0.0013	1.202	0.726

Note: Regression equation $\ln(y) = c_1 + c_2 M + c_3 \ln(R + c_4 e^{C_5 M}) \pm \sigma_{\ln y}$.

approach is to use observed ground-motion data to develop a set of empirical attenuation equations based on a semi-theoretical attenuation model. Although synthetic modeling of earthquake ground-motion (e.g., Kamae et al., 1998) and hybrid methods (e.g., Field, 2000) were also used in ground-motion predictions, the empirical method is adopted in the present study.

Table 4
Regression coefficients of attenuations for the hanging-wall and soil sites.

Period	c_1	c_2	c_3	c_4	c_5	$\sigma_{\ln y}$
PGA	−3.248	0.943	−1.471	0.100	0.648	0.628
0.01	−3.008	0.905	−1.451	0.110	0.638	0.623
0.06	−1.994	0.809	−1.500	0.251	0.518	0.686
0.09	−1.408	0.765	−1.551	0.280	0.510	0.709
0.10	−1.508	0.785	−1.551	0.280	0.500	0.713
0.20	−3.226	0.870	−1.211	0.045	0.708	0.687
0.30	−4.050	0.999	−1.205	0.030	0.788	0.657
0.40	−5.293	1.165	−1.167	0.011	0.958	0.655
0.50	−6.307	1.291	−1.134	0.0042	1.118	0.653
0.60	−7.209	1.395	−1.099	0.0016	1.258	0.642
0.75	−8.309	1.509	−1.044	0.0006	1.408	0.651
1.0	−9.868	1.691	−1.004	0.0004	1.485	0.677
1.5	−11.216	1.798	−0.965	0.0003	1.522	0.722
2.0	−12.806	2.005	−0.975	0.0005	1.528	0.759
3.0	−13.886	2.099	−1.077	0.0004	1.548	0.787
5.0	−14.606	2.160	−1.114	0.0004	1.562	0.820

Note: Regression equation $\ln(y) = c_1 + c_2 M + c_3 \ln(R + c_4 e^{C_5 M}) \pm \sigma_{\ln y}$.

Table 6
Regression coefficients of attenuations for the footwall and soil sites.

Period	c_1	c_2	c_3	c_4	c_5	$\sigma_{\ln y}$
PGA	−3.218	0.935	−1.464	0.125	0.650	0.630
0.01	−3.306	0.937	−1.454	0.100	0.670	0.626
0.06	−1.896	0.977	−1.744	0.140	0.720	0.685
0.09	−1.256	0.907	−1.754	0.151	0.720	0.708
0.10	−1.306	0.907	−1.734	0.151	0.710	0.712
0.20	−3.310	0.957	−1.291	0.100	0.700	0.690
0.30	−4.880	1.219	−1.294	0.031	0.910	0.663
0.40	−5.628	1.239	−1.181	0.0122	1.020	0.654
0.50	−6.284	1.311	−1.160	0.0057	1.130	0.652
0.60	−7.252	1.429	−1.128	0.0025	1.260	0.640
0.75	−8.355	1.536	−1.065	0.0008	1.420	0.648
1.0	−9.860	1.692	−0.995	0.0005	1.504	0.673
1.5	−11.750	1.919	−0.997	0.0005	1.544	0.714
2.0	−12.827	2.025	−0.996	0.0005	1.536	0.756
3.0	−13.795	2.069	−0.989	0.0005	1.490	0.784
5.0	−14.256	2.120	−1.144	0.0007	1.480	0.822

Note: Regression equation $\ln(y) = c_1 + c_2 M + c_3 \ln(R + c_4 e^{C_5 M}) \pm \sigma_{\ln y}$.

Commonly used attenuation models are comprised of source characteristics, geometry spreading and inelastic attenuation. When the site effect is considered, the general form becomes:

$$y = b_1 f_1(M) f_2(R) f_3(M,R) f_4(P_i)\varepsilon, \tag{2}$$

in which y is the ground-motion parameter; b_1 is a constant; $f_1(M)$ is a function relevant to magnitudes; $f_2(R)$ is a function relevant to distance; $f_3(M, R)$ is a function relevant to magnitude and distance; $f_4(P_i)$ is a function relevant to site effect; ε represents random error.

In the past, y in Eq. (2) has been mainly PGA, but for the purpose of establishing a uniform hazard response spectrum in seismic hazard analysis, y can refer also to the amplitude of the response spectrum for the structure period T. In such case Eq. (2) can be rewritten as

$$y(T) = b_1 f_1(M,T) f_2(R,T) f_3(M,R,T) f_4(P_i,T)\varepsilon(T). \tag{3}$$

To obtain this equation, data for a regression analysis are obtained by calculating a 5% critical-damping ratio response spectrum from each available earthquake record. In this study periods ranging from 0.01 s to 5 s were selected and in particular 0, 0.01, 0.06, 0.09, 0.1, 0.2, 0.3, 0.4, 0.5, 0.6, 0.75, 1.0, 1.5, 2.0, 3.0 and 5.0 s.

As attenuation model for the regression analysis, given the physical properties of the attenuation model, we adopted the functional form proposed by Campbell (1981) for analyzing the horizontal PGA, which have proved its adequacy in previous studies, i.e.:

$$ln\left(PGA_{ij}\right) = c_1 + c_2 M_i + c_3\, ln\left(R_{ij} + c_4 e^{c_5 M_i}\right) + \ ln\varepsilon, \tag{4}$$

where i denotes the ith earthquake; j denotes the jth station that recorded the ith earthquake; PGA(g) is the geometric mean of the horizontal PGA values; M is the moment magnitude; R is the closest distance (in km) to the rupture surface; ε is a random error.

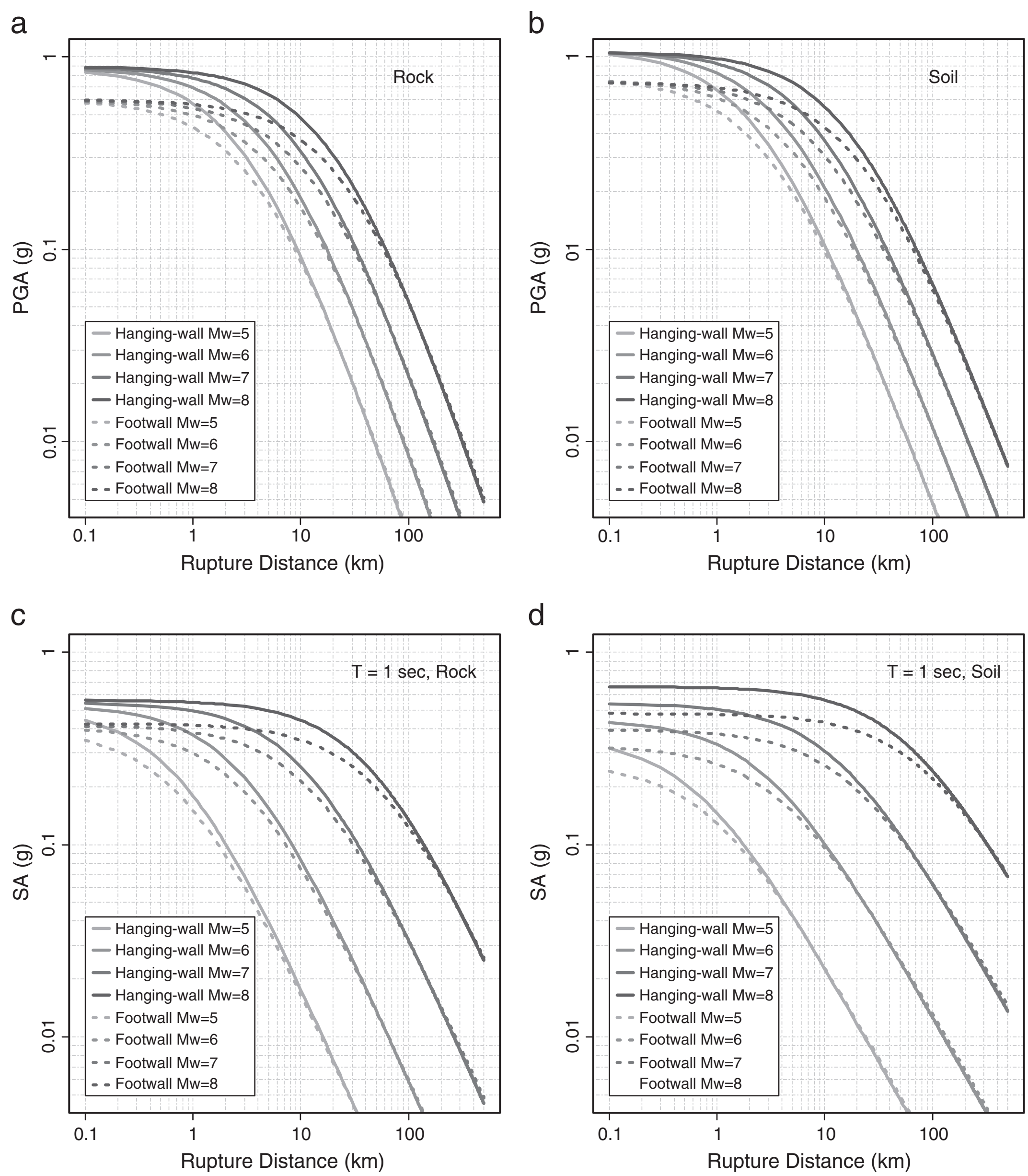

Fig. 4. Comparison of hanging-wall and footwall attenuation for different earthquake magnitudes: (a) PGA, rock sites; (b) PGA, soil sites, (c) SA at 1 s, rock sites; (d) SA at 1 s, soil sites. The difference between the hanging-wall and footwall ground-motion was in the short distance range (10–30 km).

Campbell (1981) proposed two versions of his model based on the functional form, one unconstrained, for which all the coefficients in Eq. (4) are derived from regression, and another "constrained", for which c_3 was fixed ("far field constraint") and c_5 was assumed equal to $-c_2/c_3$. The latter constraint implies that PGA assumes equal values for any magnitude as distance from rupture surface goes to zero ("total magnitude saturation"). Since we have a large data set (52 earthquakes and 5268 records), in our study we did not adopt the "far field" constraint and let the regression to determine the relative coefficient. On the contrary the "total magnitude saturation" was incorporated in our model. Our consideration is that earthquake magnitude is proportional to fault area and fault displacement, and ground motion is also proportional to fault area and fault displacement, and inversely proportional to square distance. Therefore, when distance is closing to zero, only a small area may influence the peak motion, no matter how big is the fault plane.

With regard to the response spectrum attenuation form for different periods, the functional form adopted was the same as for PGA, i.e.:

$$ln\left(SA_{ij}\right) = c_1 + c_2 M_i + c_3\, ln\left(R_{ij} + c_4 e^{c_5 M_i}\right) + ln\varepsilon. \quad (5)$$

Here SA, in g units, is the amplitude of response spectrum for each period; M, R, and ε are defined the same as for the horizontal PGA attenuation form. In this case, the unconstrained functional form of Campbell (1981) is adopted, and all the coefficients in Eq. (4) are derived from regression.

The least squares basis for the non-linear regression model (Eqs. (4) and (5)) can be formulated as

$$S = \sum_{i=1}^{n} \sum_{j=1}^{m} \left[lnY_{ij} - f\left(M_i, R_{ij}, \mathbf{C}\right)\right]^2, \quad (6)$$

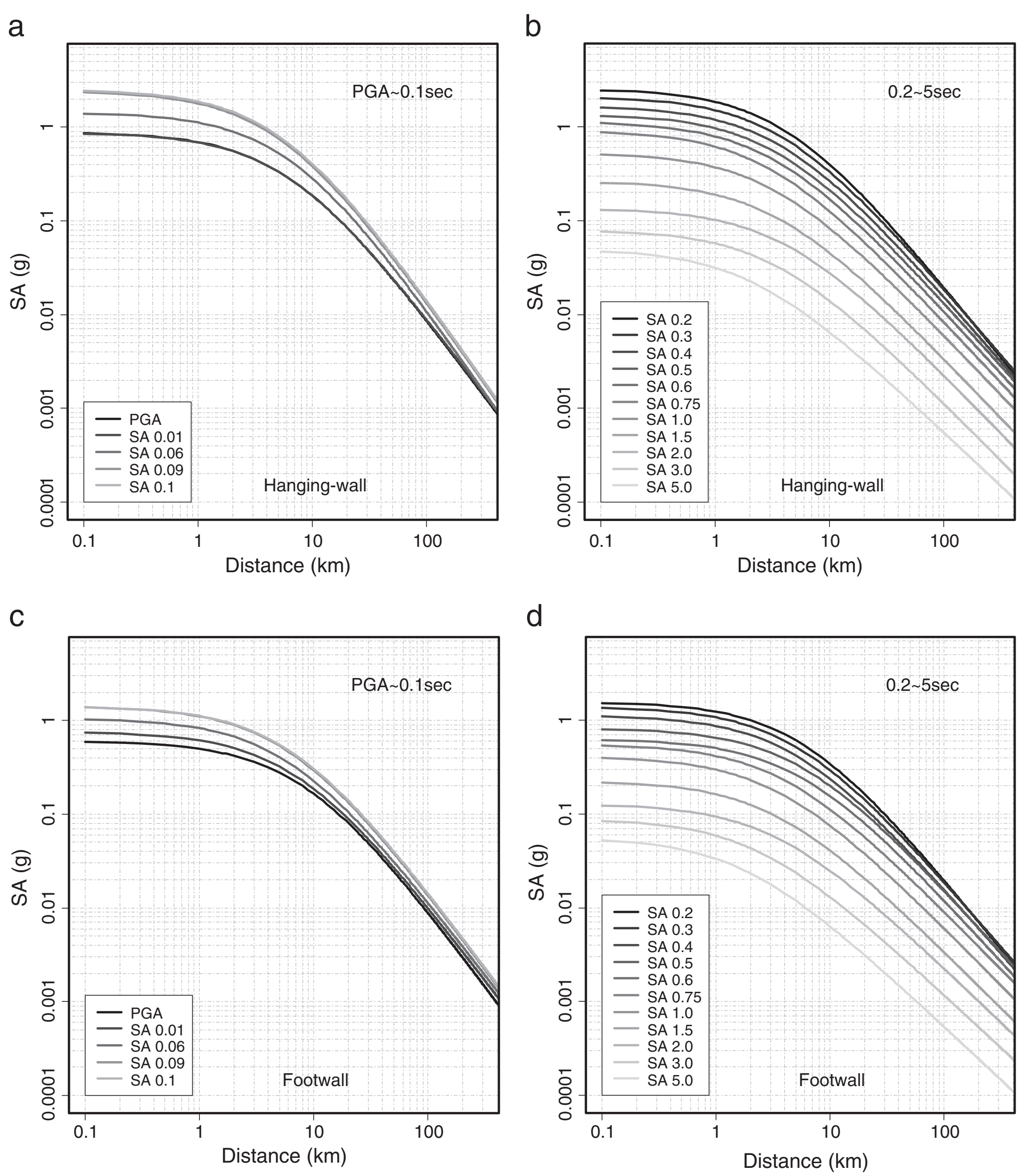

Fig. 5. Attenuation curves for rock sites at a magnitude of 6.0: (a) for PGA and SA with periods from 0.01 to 0.1 s for hanging-wall; (b) for SA with periods from 0.2 to 5.0 s for hanging-wall; (c) for PGA and SA with periods from 0.01 to 0.1 s for footwall; (d) for SA with periods from 0.2 to 5.0 s for footwall.

in which Y_{ij} is the observed ground-motion value, and $f(M_i, R_{ij}, \mathbf{C})$ is the mean value of the logarithm of the response of the ijth case following the non-linear function of Eqs. (4) and (5). The symbol $\mathbf{C}$ is a vector representing coefficients c_1, c_2, ..., c_n. In the present study, the c_1, c_2, ..., c_n values that minimize the function S were found through a numerical search method, i.e. the "block hill-climbing search" approach described in Lin and Lee (2008).

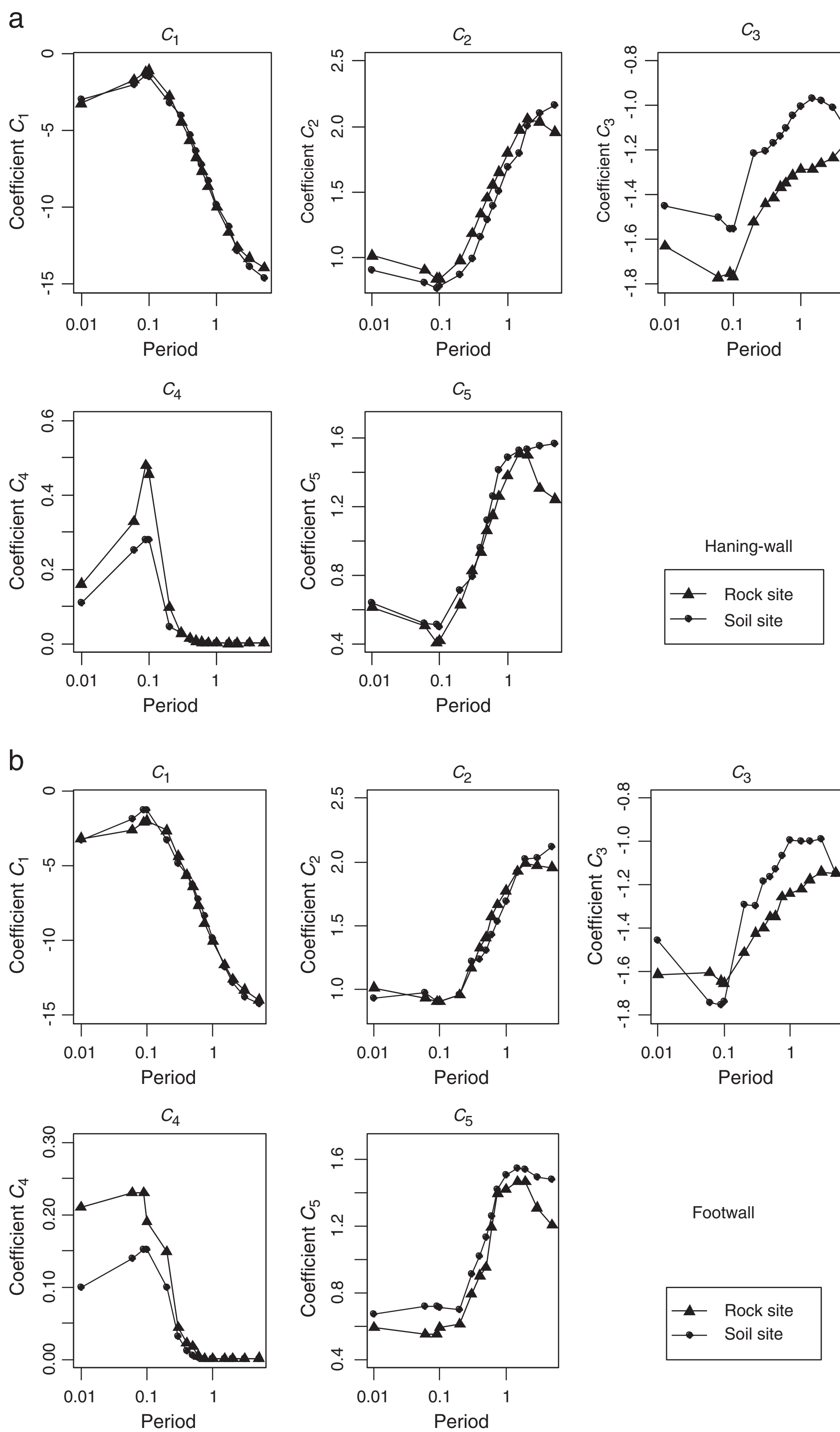

Fig. 6. Variation of coefficients (c_1–c_5) with period in the SA attenuation equations: (a) hanging-wall model; (b) footwall model.

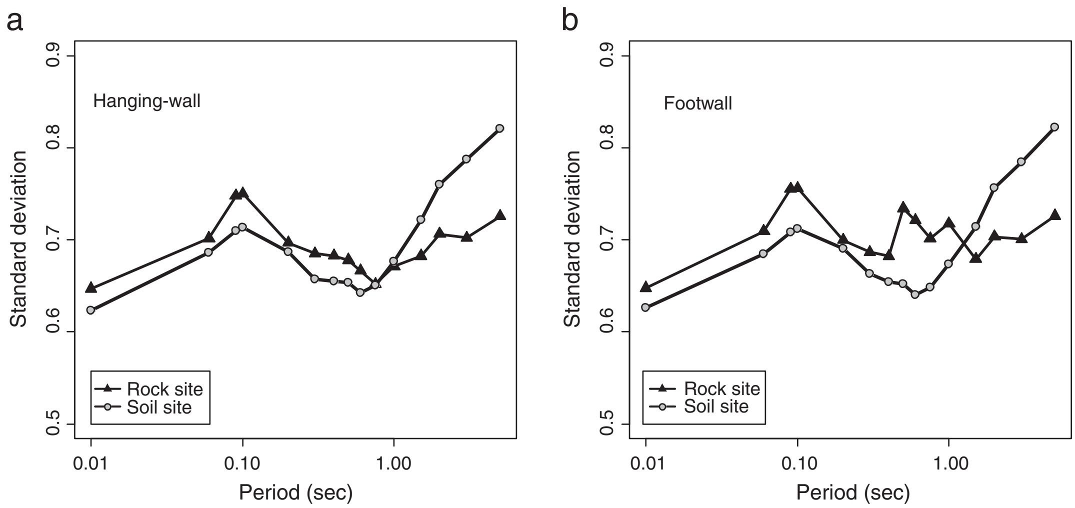

Fig. 7. Variation of the standard deviation in the SA equations for periods from 0.01 to 5.0 s for: (a) hanging-wall; (b) footwall.

5. Results

Four distinct groups of equations were obtained from regression analysis results for hanging-wall or footwall, and rock site or soil site. The obtained horizontal PGA attenuation equations are as follows:

Hanging-wall rock site:

$$\ln(\mathrm{PGA}) = -3.279 + 1.035\,M - 1.651\ln\left(R + 0.152e^{0.623M}\right); \quad (7)$$

Hanging-wall soil site:

$$\ln(\mathrm{PGA}) = -3.248 + 0.943\,M - 1.471\ln\left(R + 0.100e^{0.648M}\right); \quad (8)$$

Footwall rock site:

$$\ln(\mathrm{PGA}) = -3.232 + 1.047\,M - 1.662\ln\left(R + 0.192e^{0.630M}\right); \quad (9)$$

Footwall soil site:

$$\ln(\mathrm{PGA}) = -3.218 + 0.935\,M - 1.464\ln\left(R + 0.125e^{0.650M}\right). \quad (10)$$

In these equations, the PGA is the geometrical mean of the horizontal PGA in g, M is the moment magnitude and R is the closest distance from the rupture surface. The coefficients of the response spectrum attenuation equations for each period are tabulated in Tables 3–6; the standard deviations of the regression errors $\sigma_{\ln\varepsilon}$ (sigma) are also listed therein.

The differences between the four attenuation relations developed in this study can be seen in Fig. 4. It is clear that higher prediction of PGA values (by about 50%) are obtained for the hanging-wall attenuation relationship for rock sites at distances less than 10 km from the source (Fig. 4a). A similar difference (by about 40%) is also observed for soil sites (Fig. 4b). A comparison of the footwall PGA attenuations between rock sites and soil sites shows generally higher ground-motion values in the latter. However, since our data set is very limited for distances less than 10 km, we cannot conclusively demonstrate that at such distances soil amplification still actually exists. We also compare the differences of SA attenuation relations at a structural period of 1 s. Hanging-wall attenuation relation predict also higher values (by about 40% for both site categories), and soil-site relation shows higher ground-motion values (Fig. 4c, d). The PGA

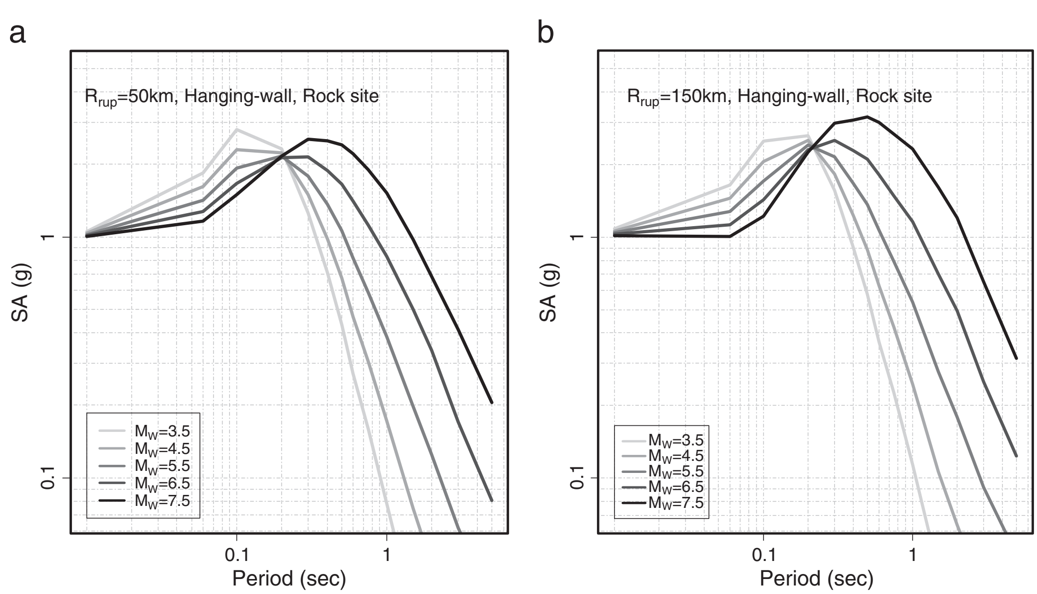

Fig. 8. Variations of normalized spectral shapes with different magnitudes for the hanging-wall and rock site model at a fixed source-to-site distance of 50 km (a) and of 150 km (b).

attenuation relations clearly show the total magnitude saturation imposed by the model (Fig. 4a, b), whereas the unconstrained SA attenuation relations do not show a similar saturation (Fig. 4c, d).

Fig. 5 presents the PGA and SA attenuation curves for rock site at M_W 6.0 for various periods. Periods of 0.1 to 0.2 s give the highest predicted values, both in the hanging-wall and footwall attenuation models.

A comparison of the coefficients of the four attenuation models obtained with the various period response spectrum attenuation equations is shown in Fig. 6. For increasing periods, coefficient c_1 increases until a period of 0.1 s and then decreases; this implies that the acceleration response spectrum values gradually decrease for longer periods. Coefficient c_2, which is related to magnitude, has the minimum at a period of 0.1 s and the maximum at a period of 5 s for soil sites and 2 s for rock sites. Coefficient c_3, which is related to the rate of attenuation with distance, shows the largest slope of about 0.1 s and a lower slope at longer periods. Coefficient c_4 has the highest value at a period close to 0.1 s, whereas coefficient c_5 at the same period has the lowest value.

The sigmas listed in Tables 3–6 are plotted against periods in Fig. 7. Their values show a general ascending trend with increasing periods. The largest value of sigma is found at the largest period on soil sites,

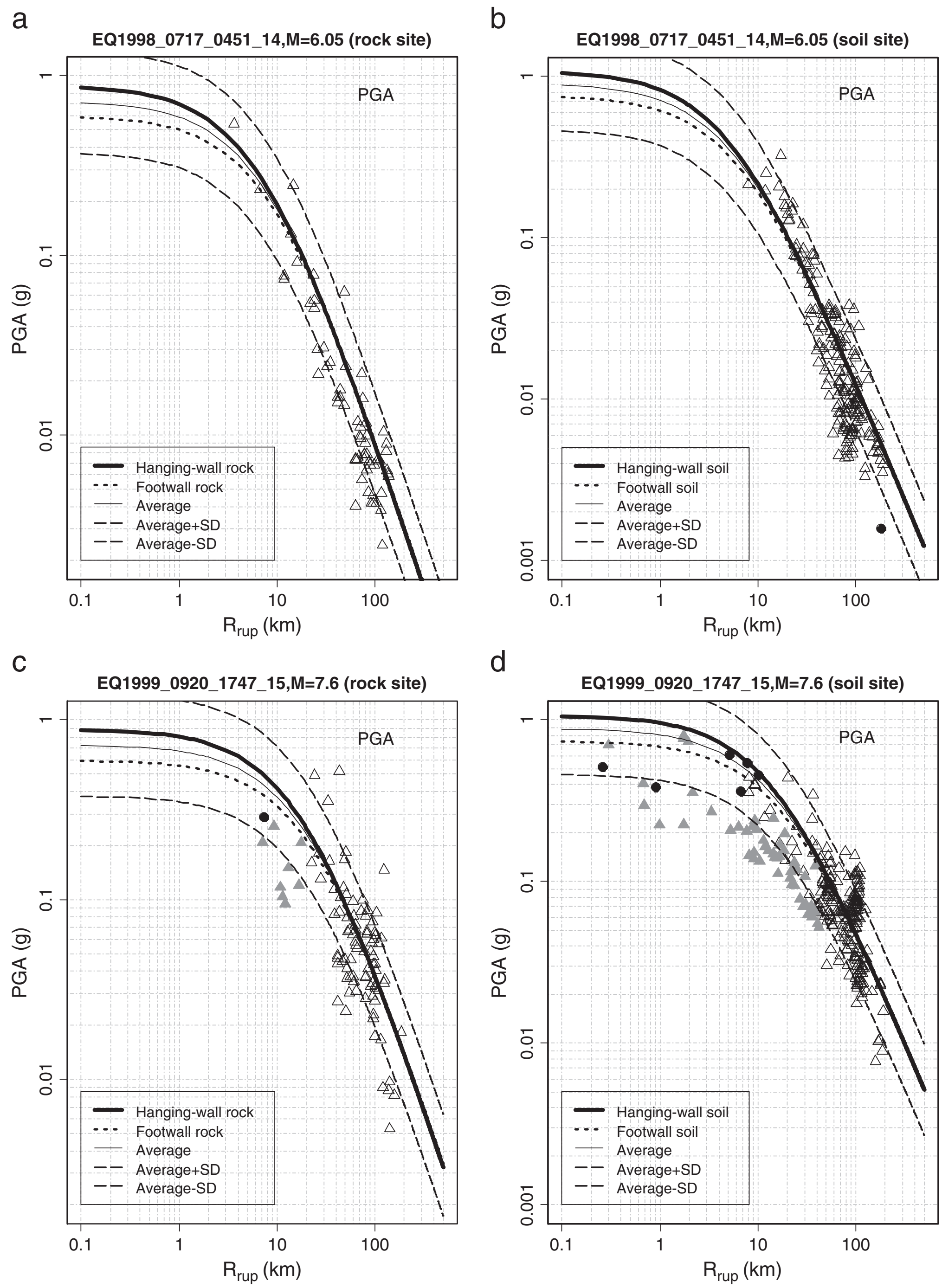

Fig. 9. Comparison of the PGA data with the median value predicted by the hanging-wall model (solid thick line), by the footwall model (dotted line) and by an average model (solid thin line) $\pm\sigma$ (dashed lines) for: (a) M_W 6.05 and rock sites; (b) M_W 6.05 and soil sites; (c) M_W 7.6 and rock sites; (d) M_W 7.6 and soil sites. Observed PGA values are represented by symbols similar to those in Fig. 3, i.e. full black circles: hanging-wall; full gray triangles: footwall; open triangles: others.

but not for the rock site cases, where the maximum is found at 0.1 s. The sigma ranges from 0.623 to 0.822. At periods larger than 2 s the soil site model gives larger sigmas than the rock site model for both the hanging-wall and the footwall conditions.

For a more detailed comparison of attenuation models with different magnitudes and distances, we plot normalized acceleration response spectrum for distances of 50 km and 150 km for hanging-wall and rock site conditions (Fig. 8). The normalization was done by dividing SAs by the PGA. The results show that the spectral acceleration increases with magnitude at periods greater than 0.2 s, but decreases for increasing magnitudes at periods smaller than 0.2 s. According to our results, the phenomena and trends for the soil sites are similar. A similar trend was also found for the subduction zone case discussed by Lin and Lee (2008).

We examine the goodness of fit of the models by plotting the observed PGA values as function of rupture distance together with the obtained attenuation curves. Fig. 9 shows the data for two typical earthquakes together with the PGA attenuation curves for the hanging-wall site model, the footwall model, the average of both models, the average plus one sigma, and the average minus one sigma.

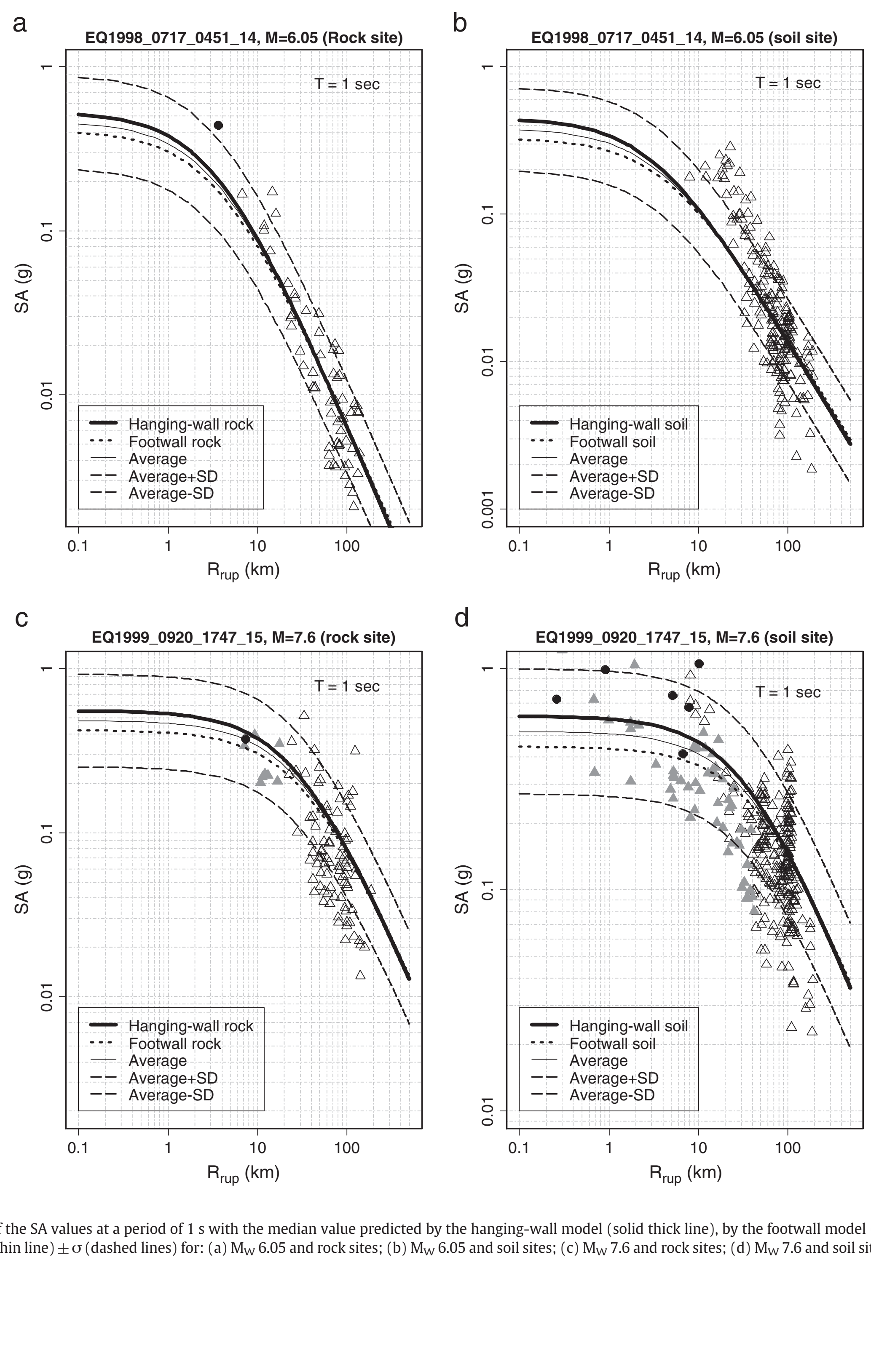

Fig. 10. Comparison of the SA values at a period of 1 s with the median value predicted by the hanging-wall model (solid thick line), by the footwall model (dotted line) and by an average model (solid thin line) $\pm\sigma$ (dashed lines) for: (a) M_W 6.05 and rock sites; (b) M_W 6.05 and soil sites; (c) M_W 7.6 and rock sites; (d) M_W 7.6 and soil sites. Symbols are similar to those in Fig. 9.

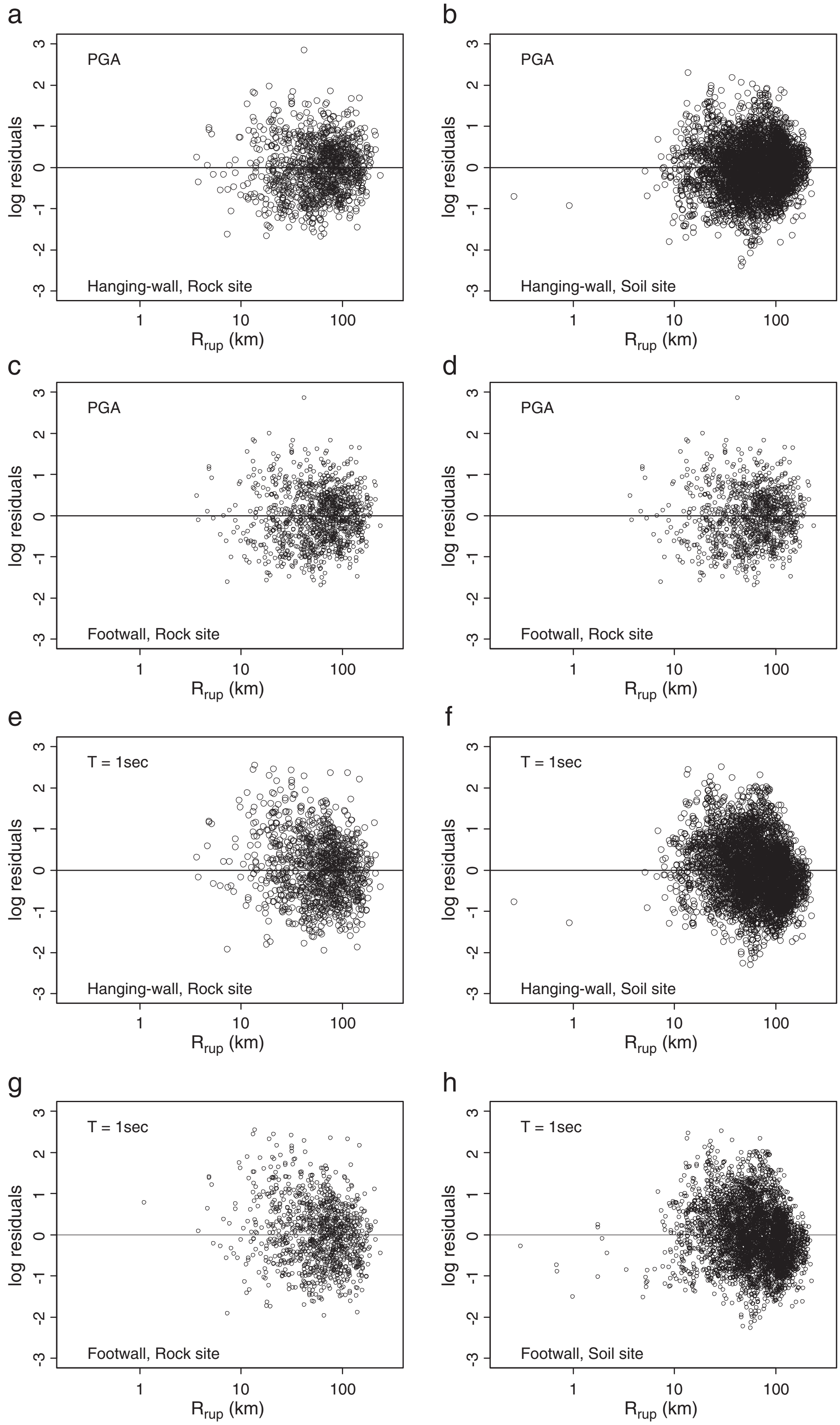

Fig. 11. Residuals for different PGA and SA attenuation equations versus distance: (a) PGA, hanging-wall, rock sites; (b) PGA, hanging-wall, soil sites; (c) PGA, footwall, rock sites; (d) PGA, footwall, soil sites; (e) SA, hanging-wall, rock sites; (f) SA, hanging-wall, soil sites; (g) SA, footwall, rock sites; (h) SA, footwall, soil sites.

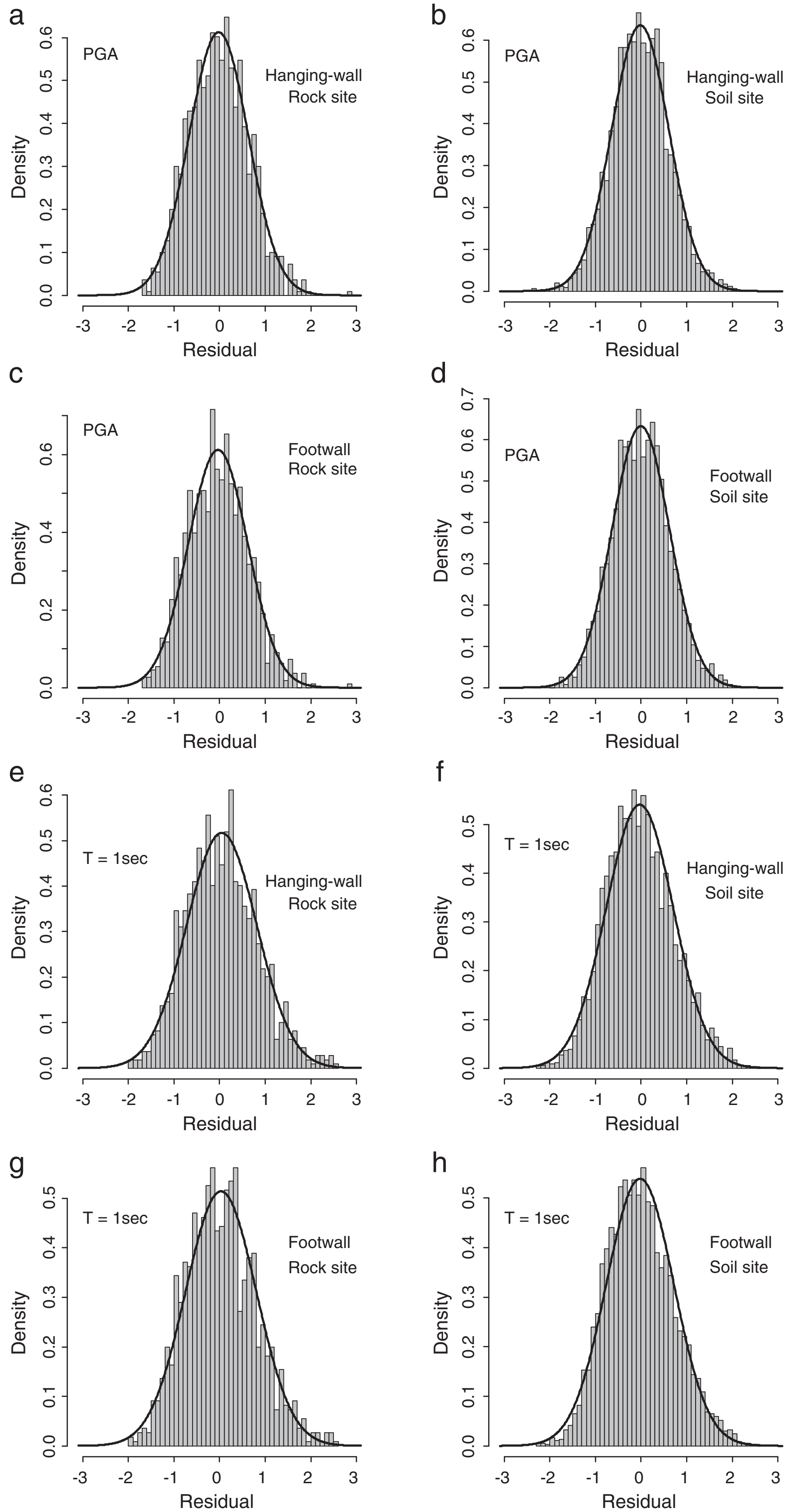

Fig. 12. Histogram of residuals of different PGA and SA attenuation equations for: (a) PGA, hanging-wall, rock sites; (b) PGA, hanging-wall, soil sites; (c) PGA, footwall, rock sites; (d) PGA, footwall, soil sites; (e) SA, hanging-wall, rock sites; (f) SA, hanging-wall, soil sites; (g) SA, footwall, rock sites; (h) SA, footwall, soil sites.

Fig. 9a and b shows the PGA values observed for an earthquake of magnitude 6.05 occurred in 1998, without the specification of site location on hanging-wall or footwall side; Fig. 9c and d show the data from the Chi-Chi earthquake for which the distinction between hanging-wall and footwall data was available. Fig. 10 shows, for the same two earthquakes, the fitting of the observed data to the SA attenuation curves at 1 s. Fig. 10a and b shows the SA values observed for the 1998 earthquake; Fig. 10c and d shows the data from the Chi-Chi earthquake. All the figures show that our model fits well the data.

To examine if there is any trend in the regression results, we plot the residual values between observed and predicted ground-motions against distance for the PGA attenuation model. As shown in Fig. 11, residuals do not exhibit any bias. A histogram plot of the residuals is shown in Fig. 12, and indicates that the residuals closely follow a log-normal distribution. These figures demonstrate the good quality of our regression results.

6. Discussion

Is it necessary to develop a local set of ground-motion attenuation equations for ground-motion predictions and PSHA application? This question may be clarified through the comparison of the results from the present study with some global sets of PGA attenuation equations (Fig. 13) and spectral attenuation equations (Fig. 14) resulted from the Next Generation Attenuation (NGA) project. Equations obtained by different authors within the framework of this project (Abrahamson and Silva, 2008; Boore and Atkinson, 2008; Campbell and Bozorgnia, 2008; Chiou and Youngs, 2008; Idriss, 2008) were compared with the Taiwan rock-site relations, adopting a Vs30 value of 760 m/s to characterize rock-sites in the NGA models. In the Taiwan case, site classes B and C are taken as rock site with Vs30 ranging from 360 m/s to more than 760 m/s. Therefore, the comparison is on the same basis or the Taiwan case is rather conservative (predicting higher ground motion values).

An examination of Fig. 13 shows that the Taiwan PGA set is similar to that of the NGA attenuation equations for distances less than about 20 km. However, it is significantly lower than that of the NGA attenuation equations for distances greater than 20 km. The steeper slope of the Taiwan attenuation curves could be due to the fact that Taiwan is a very young orogen, so that the crust is weak and Q values are low (Wang et al., 2003). This implies a relatively high attenuation, especially for high-frequency waves.

This is confirmed by the observation that, for structural periods shorter than 0.3 s, the spectral accelerations obtained in this study are significantly lower than those of NGA's equations. On the contrary, for periods longer than 0.3 s, they are more similar to (Fig. 14a) or a little bit lower (Fig. 14b) than in NGA models. This indicates that a local set of ground-motion attenuation equations could be needed for deriving more accurate ground-motion prediction. This is particularly important for a correct definition of design spectra of small building with a limited number of stores (i.e. with resonance frequency higher than 3 Hz).

Lin and Lee (2008) also obtained a lower ground-motion prediction in their subduction zone earthquake results than that of global sets. They obtained a significantly lower PGA value for periods of less than 0.3 s, and not so different values for periods greater than 0.3 s (Lin and Lee, 2008, Figure 17). This suggests that both shallow crustal earthquake sources and subduction zone earthquake sources have similar attenuation patterns for wave propagation through a low-Q young orogen.

Ten years ago, a California consulting company predicted a 475-year return time PGA level of 0.47 g for downtown Taipei (Chiou et al., 2001). This caused a big shock to seismologists and earthquake engineers in Taiwan, because this value is twice as large as the building code value in Taipei. We examined the report and the paper of Chiou et al. (2001), and realized that 4 set of California crustal attenuation equations (Abrahamson and Silva, 1997; Boore et al., 1997; Campbell, 1997; Sadigh et al., 1997) and a global set of subduction zone attenuation equations (Youngs et al., 1997) had been used in the PSHA. We thought that the key to explain their results might be the use of attenuation equations not proper for the Taipei case, and we started to develop local attenuation equations. A recent study (Cheng et al., 2010) revising those results predicted a 475-year PGA level of 0.30 g for downtown Taipei, using the same source data but different attenuation equations, i.e. the shallow crustal attenuation equations presented in this study and the subduction zone attenuation equations of Lin and Lee (2008). In other words, using a local set of attenuation equations for the PSHA reduced the PGA level by 42% in the Taipei case.

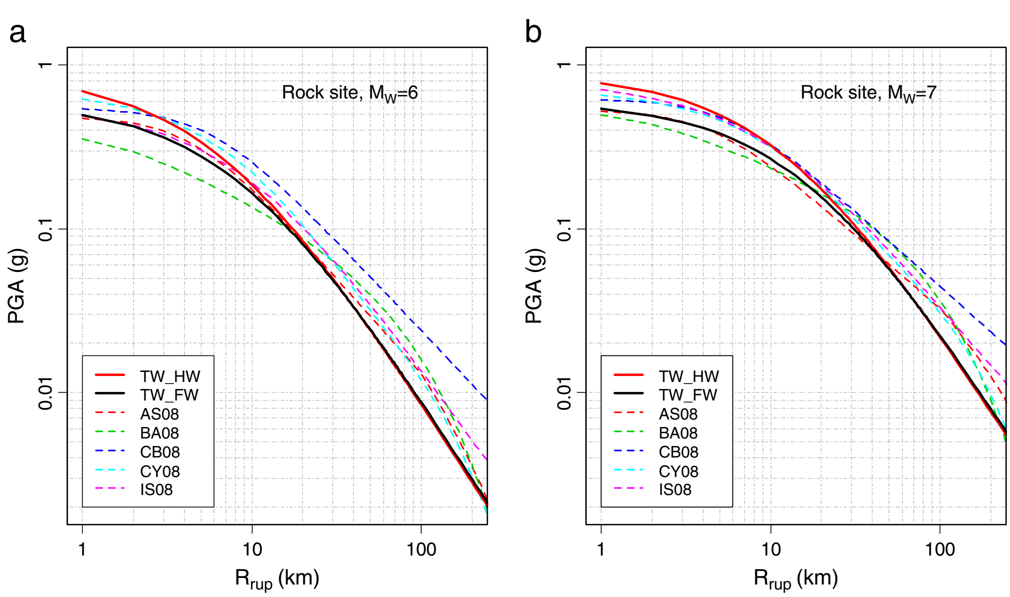

Fig. 13. Comparison of the PGA attenuation curves from results obtained in this study and some global sets for: (a) M_W 6; (b) M_W7. Solid red and black lines indicate hanging-wall and footwall models of present study, respectively. The other curves are relative to the following relations: AS08, Abrahamson and Silva (2008); BA08, Boore and Atkinson (2008); CB08, Campbell and Bozorgnia (2008); CY08, Chiou and Youngs (2008); IS08, Idriss (2008).

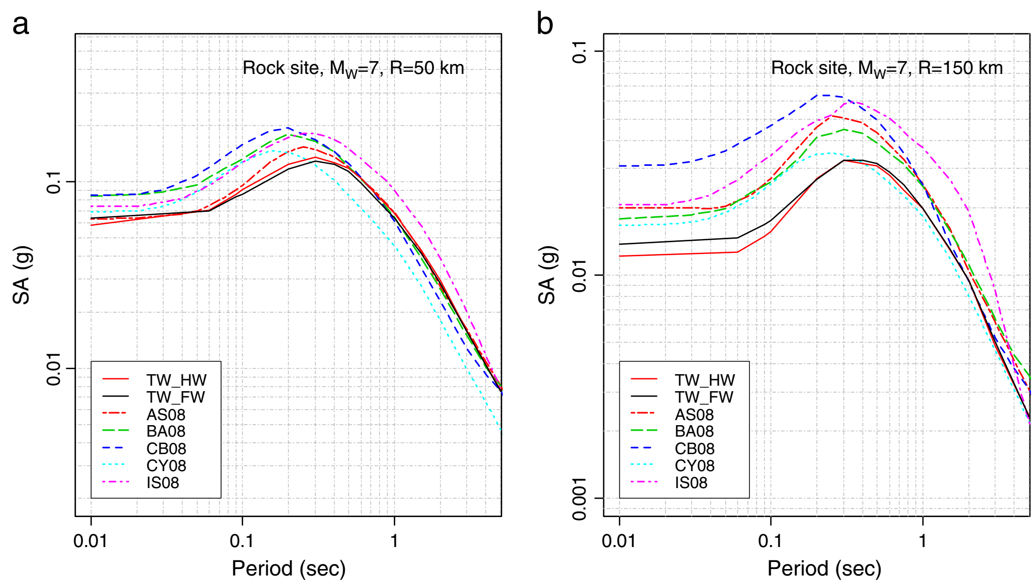

Fig. 14. Comparison of spectral acceleration predicted by this study and some global sets for: (a) M_W 7 and distance 50 km, (b) M_W 7 and distance 150 km. Definition for line styles and colors is the same as in the previous figure.

It is now generally accepted that ground-motion scales non-linearly with magnitude. We have plotted data vs. magnitude to examine the model we used. Results reveal that the present model also scale non-linearly with magnitude and the observed data fit good with the model within the data range between M_W 3.5 and M_W 7.6 (Fig. 15)

Plotting SA vs. distance for long-period spectra of 3 typical earthquakes (Fig. 16), results reveal that most data fit the median attenuation curve. However, in our database, only the Chi-Chi mainshock has plenty of near field data and shows distance saturation. Other earthquakes are still lacking for near field data so that the occurrence of magnitude saturation phenomenon cannot be evaluated from the available data. We believe there are still rooms for discussion of magnitude saturation at long periods and this topic needs more studies in the future.

Although several studies have shown that soil motion tends to be de-amplified under large strain, the obtained equations predict significant soil amplification also under such conditions. However, in Fig. 9d, it is clear that our equations over-predict the soil PGA from Chi-Chi earthquake for rupture distance less than 20 km. Neverthe-less, this over-prediction feature is not seen in SA at 1 s as shown in Fig. 10d. Soil de-amplified under large strain and for short periods may be considered in the future studies.

7. Conclusions and recommendations

A set of response spectral attenuation equations, including PGA and SAs with structural periods of up to 5.0 s, for both hanging-wall

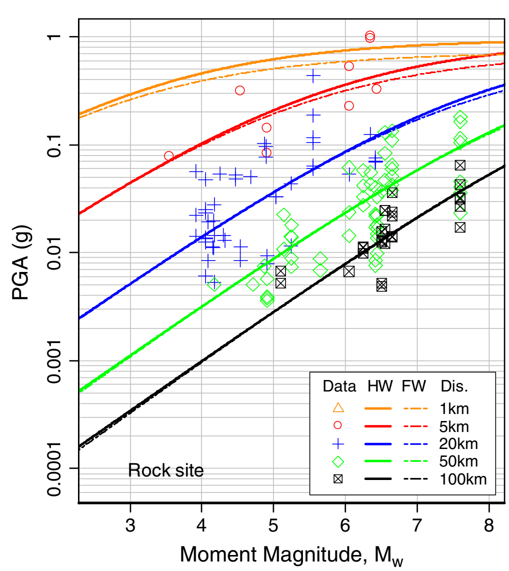

Fig. 15. Plot of PGA data vs. magnitude observed at different distances (represented with different colors), showing nonlinear magnitude scaling (buffer zone for distance is 2 km). Solid and dashed lines represent the values predicted by the obtained attenuation relations for hanging-wall and footwall sites, respectively.

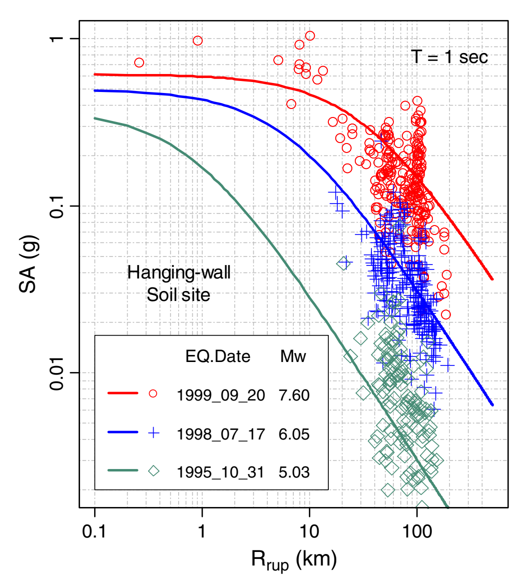

Fig. 16. SA data vs. distance plot for 3 typical earthquakes (represented with different colors), showing distance saturation and possible magnitude saturation at long period. The legend reports date and moment magnitude (M_w) of the three earthquakes.

and footwall models and rock and soil sites, for Taiwan shallow crustal earthquakes, has been completed. The obtained attenuation equations give higher ground-motion estimates for the hanging-wall than for the footwall side, and higher ground-motion estimates for soil sites than for rock site. These attenuation equations should provide better ground-motion estimates for Taiwan, and make it possible to construct a uniform hazard response spectrum from PSHA.

The results confirm that the local set of attenuation equations gives lower predicted PGA values than global sets for distances greater than 20 km. The steeper slope of the Taiwan attenuation curves could be due to the fact that, Taiwan being a very young orogen, the crust is weak and has low Q values. The spectral accelerations obtained in this study are also lower than those obtained with the global sets for structural periods shorter than 0.3 s, but are similar to those of global sets for longer periods. The development of a local set of ground-motion attenuation equations is necessary for more accurate prediction of ground-motion values. This would be of great assistance in engineering planning, design, and safety evaluation of existing structures in the Taiwan region.

In the use of this local set of ground-motion attenuation equations, the hanging-wall sets and the footwall sets may be combined and an average value may be used in case of strike-slip earthquake or if an earthquake is not expected to rupture or to deform the ground surface.

Acknowledgments

We extend our deepest thanks to the Seismology Center of the Central Weather Bureau of Taiwan for providing the strong-motion data. The manuscript was greatly improved based on the comments and suggestions made by the anonymous reviewers. This research was supported by the Taiwan Earthquake Research Center (TEC) funded through the National Science Council (NSC) under Grant Number NSC96-2119-M-008-004.

References

Abrahamson, N.A., Silva, W.J., 1997. Empirical response spectra attenuation relations for shallow crustal earthquakes. Seismological Research Letters 68 (1), 94–127.
Abrahamson, N.A., Silva, W.J., 2008. Summary of the Abrahamson & Silva NGA ground-motion relations. Earthquake Spectra 24, 67–97.
Anderson, J., Brune, J., 1999. Probabilistic seismic hazard assessment without the ergodic assumption. Seismological Research Letters 70, 19–28.
Beresnev, I.A., Atkinson, G.M., 1999. Generic finite-fault model for ground-motion prediction in eastern North America. Bulletin of the Seismological Society of America 89, 608–625.
Bommer, J.J., Abrahamson, N., 2006. Why do modern probabilistic seismic-hazard analyses often lead to increase hazard estimates? Bulletin of the Seismological Society of America 96, 1967–1977.
Boore, D.M., Atkinson, G.M., 2008. Ground-motion prediction equations for the average horizontal component of PGA, PGV, and 5%-damped PSA at spectral periods between 0.01 s and 10.0 s. Earthquake Spectra 24, 99–138.
Boore, D.M., Joyner, W.B., Fumal, T.E., 1997. Equations for estimating horizontal response spectra and peak acceleration from western North America earthquakes: a summary of recent work. Seismological Research Letters 68 (1), 128–153.
Bonilla, M.G., 1975. A review of recently active faults in Taiwan. U. S. Geological Survey Open File Report 75-41.
Bonilla, M.G., 1977. Summary of Quaternary faulting and elevation changes in Taiwan. Geological Society of China Memoir 2, 43–55.
Bowin, C., Lu, R.S., Lee, C.S., Schouten, H., 1978. Plate convergence and accretion in the Taiwan–Luzon region. American Association of Petroleum Geologists bulletin 62, 1645–1972.
Campbell, K.W., 1981. Near-source attenuation of peak horizontal acceleration. Bulletin of the Seismological Society of America 71, 2039–2070.
Campbell, K.W., 1997. Empirical near-source attenuation relationships for horizontal and vertical components of peak ground acceleration, peak ground velocity, and pseudo-absolute acceleration response spectra. Seismological Research Letters 68, 154–179.
Campbell, K.W., Bozorgnia, Y., 2008. NGA ground motion model for the geometric mean horizontal component of PGA, PGV, PGD and 5% damped linear elastic response spectra for periods ranging from 0.01 to 10 s. Earthquake Spectra 24, 139–171.
Chai, B.H.T., 1972. Structure and tectonic evolution of Taiwan. American Journal of Science 272, 389–422.
Chang, T.Y., Cotton, F., Angelier, J., 2001. Seismic attenuation and peak ground acceleration in Taiwan. Bulletin of the Seismological Society of America 91, 1229–1246.
Cheng, C.T., Lee, C.T., Lin, P.S., Lin, B.S., Tsai, Y.B., Chiou, S.J., 2010. Probabilistic earthquake hazard in metropolitan Taipei and its surrounding regions. Terrestrial, Atmospheric and Oceanic Sciences 21 (3), 429–446.
Chiou, B.S., Youngs, R.R., 2008. An NGA model for the average horizontal component of peak ground motion and response spectra. Earthquake Spectra 24, 173–215.
Chiou, S.J., Cheng, C.T., Wessling, J., Chang, C.Y., 2001. Probabilistic earthquake hazard in Taipei and surrounding regions. North American Taiwan Engineers' Association (NATEA), pp. 38–45.
Dadson, S.J., Hovious, N., Chen, H., Dade, B.W., Hsieh, M.L., Willett, S.D., Hu, J.C., Horng, M.J., Chen, M.C., Stark, C.P., Lague, D., Lin, J.C., 2003. Links between erosion, runoff variability, and seismicity in the Taiwan orogen. Nature 426, 648–651.
Field, E.H., 2000. A modified ground-motion attenuation relationship for southern California that accounts for detailed site classification and a basin-depth effect. Bulletin of the Seismological Society of America 90 (6B), S209–S221.
Hanks, T.C., Kanamori, H., 1979. A moment magnitude scale. Journal of Geophysical Research 84, 2348–2350.
Heaton, T., Tajima, F., Mori, A.W., 1986. Estimating ground motions using recorded accelerograms. Surveys in Geophysics 8, 25–83.
Hsu, M.T., 1971. Seismicity of Taiwan and some related problem. Bulletin of the International Institute of Seismology and Earthquake Engineering 8, 41–160.
Hsu, M.T., 1983. Magnitude and intensity assessment of disastrous earthquakes in Ming and Ching period. Meteorological Bulletin, Central Weather Bureau 29 (4), 1–18 (in Chinese).
Hwang, J.Y., 1995. Characteristics of Strong Ground and Analysis of Seismic Hazard in Taiwan area. M.S. thesis, National Central University, Taiwan. (in Chinese with English Abstract).
Idriss, I.M., 2008. An NGA empirical model for estimating the horizontal spectral values generated by shallow crustal earthquakes. Earthquake Spectra 24, 217–242.
Kamae, K., Irikura, K., Pitarka, A., 1998. A technique for simulating strong ground motion using hybrid Green's function. Bulletin of the Seismological Society of America 88, 357–367.
Kao, H., Chen, W.P., 2000. The Chi-Chi earthquake sequence: active out-of-sequence thrust faulting in Taiwan. Science 288, 2346–2349.
Lee, C.T., Cheng, C.T., Liao, C.W., Tsai, Y.B., 2001. Site classification of Taiwan free-field strong-motion stations. Bulletin of the Seismological Society of America 91, 1283–1297.
Lee, W.H.K., Wu, F.T., Jacobsen, C., 1976. A catalog of historical earthquakes in China compiled from recent Chinese publications. Bulletin of the Seismological Society of America 66, 2003–2016.
Letouzey, J., Kimura, M., 1986. The Okinawa trough: Genesis of a back-arc basin developing along a continental margin. Tectonophysics 125, 209–230.
Lin, P.S., Lee, C.T., 2008. Ground-motion attenuation relationships for subduction-zone earthquakes in Northeastern Taiwan. Bulletin of the Seismological Society of America 98, 220–240.
Liu, K.S., 1999. Attenuation Relations for Strong Seismic Ground Motion in Taiwan. Ph.D. thesis, National Central University, Taiwan. (in Chinese with English abstract).
Liu, K.S., Shin, T.C., Tsai, Y.B., 1999. A free field strong motion network in Taiwan: TSMIP. Terrestrial, Atmospheric and Oceanic Sciences 10, 377–396.
Loh, C.H., Lee, Z.K., Wu, T.C., Peng, S.Y., 2000a. Ground motion characteristics of the Chi-Chi earthquake of 21 September 1999. Earthquake Engineering and Structural Dynamics 29 (6), 867–897.
Loh, C.H., Wen, K.L., Jean, W.Y., Chai, J.F., Teng, T.J., Rau, R.J., 2000b. The seismic force requirements considering near-fault effect and uniform hazard. Architecture and Building Research Institute, Ministry of Interior Affair, R.O.C. (in Chinese).
Ma, K.F., Lee, C.T., Tsai, Y.B., Shin, T.C., Mori, J., 1999. The Chi-Chi, Taiwan earthquake: large surface displacements on an inland fault. EOS Trans, American Geophysical Union 80 (50), 605–611.
Sadigh, K., Chang, C.Y., Egan, J.A., Makdisi, F.I., Youngs, R.R., 1997. Attenuation relationships for shallow crustal earthquakes based on California strong motion data. Seismological Research Letters 68 (1), 180–189.
Seno, T., 1977. The instantaneous rotation vector of the Philippine Sea plate relative to Eurasian plate. Tectonophysics 42, 209–226.
Seno, T., Stein, S., Gripp, A.E., 1993. A model for the motion of the Philippine Sea Plate consistent with NUVEL-1 and geological data. Journal of Geophysical Research 98 (B10), 17941–17948.
Tsai, Y.B., 1986. A study of disastrous earthquakes in Taiwan, 1683–1895. Bulletin of the Institute of Earth Sciences, Academia Sinica 5, 1–44.
Tsai, C.C., Loh, C.H., Yeh, Y.T., 1987. Analysis of earthquake risk in Taiwan based on seismotectonic zones. Memoir of Geological Society of China 9, 413–446.
Tsai, Y.B., Teng, T.L., Chiu, J.M., Liu, H.L., 1977. Tectonic implications of the seismicity in the Taiwan region. Memoir of the Geological Society of China 2, 13–41.
Tsai, Y.B., Wen, K.L., 1999. Compilation of a uniform catalog of earthquakes in Taiwan and development of motion attenuation relationships. Report of national science and technology program for hazards mitigation, NAPHM 87-07.
Wang, Y., Ma, K.F., Mooney, W.D., 2003. Shear-wave seismic attenuation in southern California and Taiwan: a comparison. EOS Trans, American Geophysical Union 84, p46.
Wu, F.T., 1978. Recent tectonics of Taiwan. Journal of Physics of the Earth 26, 265–299 (Suppl).
Wu, Y.M., Shin, T.C., Chang, C.H., 2001. Near real-time mapping of peak ground acceleration and peak ground velocity following a strong earthquake. Bulletin of the Seismological Society of America 91, 1218–1228.
Wu, Y.M., Zhao, L.C., Chang, C.H., Hsu, Y.J., 2008. Focal mechanism determination in Taiwan by genetic algorithm. Bulletin of the Seismological Society of America 98, 651–661.
Youngs, R.R., Chiou, S.J., Silva, W.J., Humphrey, J.R., 1997. Strong ground motion attenuation relationships for subduction zone earthquakes. Seismological Research Letters 68, 58–73.
Yu, S.B., Chen, H.Y., Kuo, L.C., 1997. Velocity field of GPS stations in the Taiwan area. Tectonophysics 274, 41–59.